REPORT DOCUMENTATION PAGE

Form Approved
OMB No. 0704-0188

1. REPORT DATE *(DD-MM-YYYY)*	2. REPORT TYPE	3. DATES COVERED *(From - To)*
	Final Report	01 September 2001 - 31 August 2004

4. TITLE AND SUBTITLE

Multifunctional Structural Ceramics with Ferroelastic and Martensitic Transformations

5a. CONTRACT NUMBER

5b. GRANT NUMBER

F49620-01-1-0500

5c. PROGRAM ELEMENT NUMBER

6. AUTHOR(S)

Dr. A Sayir

5d. PROJECT NUMBER

5e. TASK NUMBER

5f. WORK UNIT NUMBER

7. PERFORMING ORGANIZATION NAME(S) AND ADDRESS(ES)
Case Western Reserve University
10900 Euclid Avenue
Cleveland OH 44106

8. PERFORMING ORGANIZATION REPORT NUMBER

9. SPONSORING/MONITORING AGENCY NAME(S) AND ADDRESS(ES)
USAF/AFRL
AFOSR 875 N. Randolph Street
Arlington VA 22203
Dr. Joan Fuller/NA

10. SPONSOR/MONITOR'S ACRONYM(S)

AFOSR

11. SPONSOR/MONITOR'S REPORT NUMBER(S)

12. DISTRIBUTION/AVAILABILITY STATEMENT

Distribution Statement A. Approved for public release; distribution is unlimited.

AFRL-SR-AR-TR-06-0311

13. SUPPLEMENTARY NOTES

14. ABSTRACT
This program had 2 objectives that were pursued simultaneously. These objectives were: (i) development of process models designed to produce a new family of tough and novel ceramic materials with specific microstructures and (ii) coordinate the findings of the proposed research with the parallel efforts on the material characterization addressed from the atomistic and continuum length scales, where correlations are made between atomic structure and bonding. It was concluded that the growth of single crystal mullite is controlled by kinetics and is a non-equilibrium process. Liquid-liquid immiscibility and slow diffusion rate of cations did not permit the growth of 3:2 mullite single crystals. Using numerical modeling, we investigated the solidification of representative oxide crystals. The interactive effects of radiative heat transfer and convection on solidification of oxide crystals was experimentally investigated and isolated numerically in order to optimize the growth conditions for solidification of the materials. A combined conduction convection radiation model of solidification was developed for the oxide crystals which are transparent to radiation below wavelength of 6 micron and opaque to radiation in the rest of the spectrum.

15. SUBJECT TERMS

16. SECURITY CLASSIFICATION OF:			17. LIMITATION OF ABSTRACT	18. NUMBER OF PAGES	19a. NAME OF RESPONSIBLE PERSON
a. REPORT	b. ABSTRACT	c. THIS PAGE			
U	U	U	UU	28	19b. TELEPHONE NUMBER *(Include area code)*

Standard Form 298 (Rev. 8/98)
Prescribed by ANSI Std. Z39.18

FINAL REPORT

For the Grant

Multifunctional Structural Ceramics with Ferroelastic and Martensitic Transformations

F49620-01-1-0500

Submitted to

Dr. Joan Fuller

Air Force Office of Scientific Research

By

Dr. A. Sayir

CASE WESTERN RESERVE UNIVERSTY

20060727329

Multifunctional Structural Ceramics with Ferroelastic and Martensitic Transformations

Executive Summary

This program had two objectives that were pursued simultaneously. These objectives were: (i) development of process models designed to produce a new family of tough and novel ceramic materials with specific microstructures and (iii) coordinate the finding of the proposed research with the ongoing parallel efforts on the material characterization addressed from the atomistic and continuum length scales, where correlations are made between atomic structure and bonding. This final report summarizes the findings of PI Dr. A. Sayir of Case Western Reserve University and contains new information relating development of process models designed to produce a new mullite single crystal. It was concluded that the growth of single crystal mullite is controlled by kinetics and it is a non-equilibrium process. Liquid-liquid immiscibility and and slow diffusion rate of cations did not permit the growth of 3:2 mullite single crystals. We investigated through numerical modeling effort for solidification of representative important oxide crystals, $2Al_2O_3 \cdot SiO_2$ mullite, by the vertical Bridgman technique. The interactive effects of radiative heat transfer and convection on solidification of $2Al_2O_3 \cdot SiO_2$ was investigated experimentally and isolated numerically in order to optimize the growth conditions for solidification of the materials. A combined conduction-convection-radiation model of solidification was developed for the oxide crystals, which are transparent to radiation below wavelength of 6 μm, and opaque to radiation in the rest of the spectrum.

Mullite exhibits remarkable thermo-mecahnical stability Crystal grown from melt show a higher degree of oxygen vacancy ordering and resistance to dislocation motion. Columns of O_c are not randomly distributed along [3-10]. Vacancy rich colums tend to form ordered domains with super lattice dimensions (planes $\pm 1/3$, ± 1, ½ and $\pm 2/3, \pm 2$, ½). Vacancy rich colums are frequently seen along [131] and [261]. Simplistic model proposed and compared with the electron optic results. Aluminum and silicon occupied tetrahedral site whereas Al also had octahedral site occupancy. Model did not reflect the loss in oxygen. It was concluded that the modeling of the structure of $2Al_2O_3 \cdot SiO_2$ mullite required refined simulations using supercell to describe the periodicity of vacancies.

In a parallel study Co-PI Prof. W. Kriven of University of Illinois at Urbana-Champaign investigated martensitc toughnening mechanisms. Toughening mechanisms include transformation toughening (e.g., with zirconia, ΔV = positive), and transformation weakening causing debonding of interphases (e.g., cristobalite, enstatite, ΔV = negative). The role of unit cell shape changes remains relatively unexplored, and can lead to ferroelastic domain rearrangements, large force actuation or shape memory ceramics. Basic science research was conducted to identify, and crystallographically characterize, potentially new martensitic phase transformations in yttrium niobate ($YNbO_4$) and dysprosium titanate ($DyTiO_5$), as examples of model systems for academic understanding, as well as potentially technologically useful ceramics. A unique, newly-built, quadrupole lamp furnace capable of temperature over 2400 °C in air, in conjunction with synchrotron radiation enabled *in situ* studies.

<u>Nomenclature</u>

A	= surface area, (m^2)
Bi	= Biot number, (hR / K$_a$)
C	= specific heat, (J / kg K)
F	= radiation function
Gr	= Grashof number, (g$_0\beta$R^{3}T$_h$ / v^2)
K	= thermal conductivity, (W / m K)
	= unit normal vector
N_s	= radiation-conduction number, (σT$_h^3$R / K$_s$)
N_a	= crucible radiation-conduction number, (σT$_h^3$R / K$_a$)
Pr	= Prandtl number, (v/α)
q	= dimensionless radiative flux, $(\overline{q}/\sigma T_h^4)$
R	= radius, (m)
T	= temperature, (K)
$\overset{\text{\textasciicircum}}{\nabla}$	= Velocity Vector, $\left(\dfrac{\overline{V}}{(Gr)^2}\right)$

Greek

λ, λ_c	= wavelength, cut-off wavelength, (microns)
μ	= dynamic viscosity, (N sec / m^2)
ν	= Kinematic viscosity, (N sec / m^2)
ρ	= density, (kg / m^3)
σ	= Stefan Boltzmann constant, (W / m^2 K^4)
θ	= dimensionless Temperature (T / T$_h$)
β	= expansion coefficient, (1 / K)
ε	= emissivity

Subscripts

a	= crucible
c	= cold zone
h	= hot zone
l	= melting point
s	= crystal
r	= radial
z	= axial
∞	= ambient parameter

Radiation View Factors

$\overline{WW}$	= wall-to-wall radiation exchange factor
$\overline{WS}$	= wall-to-interface radiation exchange factor
$\overline{SW}$	= interface-to-wall radiation exchange factor
$\overline{SS}$	= interface-to-interface radiation exchange factor

1. INTRODUCTION

The brittleness of ceramics for structural applications continues to be a difficult and unsolved problem, particularly at high temperatures and in oxidizing environments. The high specific strength and stiffness of ceramic materials offers great promise in high temperature applications. Research to improve reliability, either through composite or bulk toughening, has yet to develop viable competitors to the high temperature metallic super-alloys. However, an increase in fracture toughness could make ceramic matrix composites a desirable

Fig. 1 (001) projection

alternative. There are no alternative materials to ceramics for high temperature applications. At present, the interface between engineering design and materials science currently consists of a collection of empirically developed and marginally verified material properties obtained by *ad hoc* experiments. These are laborious, time consuming and expensive. They could however, be accelerated and much for efficiently carried out with the help of information gained from model experiments providing information about the relevant features of each single component. In particular, if one understand *how* a phase transformation occurs and under what conditions it can be manipulated, a ceramic materials designer would be an a much better position to expediently design a composite which takes advantage of the phase transformation. We selected $2Al_2O_3 \cdot SiO_2$ mullite as a case study. The motivation for the selection of mullite was related to

its exceptional deformation resistance at very high temperatures. Mullite has a very complex structure as shown in Fig. 1. Yet, the exceptional resistance to plastic deformation at temperatures exceeding 1500 °C can not be explained by the complexity of the structure. The resistance to deformation does not scale with the melting tmperature as is the case for most oxides. The anticipated theoretical defct chemistry reactions are shown in Fig. 2 for x values 0,25 and 0.4, corresponding to 3:2 and 2:1 mullite.

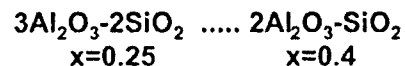$$Mullite: 2Si^{4+} \rightarrow 2Al^{3+} + V^{\cdot\cdot}_O$$

$$Al_2(Al_{2+2x}Si_{2-2x})O_{10-x}$$

$$3Al_2O_3\text{-}2SiO_2 \quad ..... \quad 2Al_2O_3\text{-}SiO_2$$
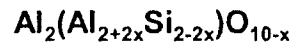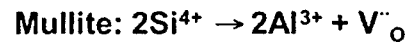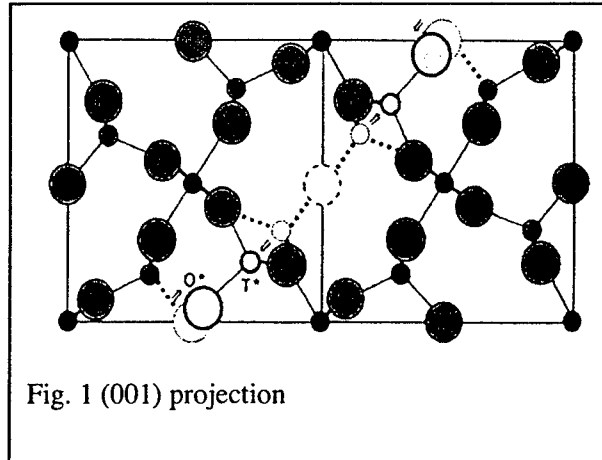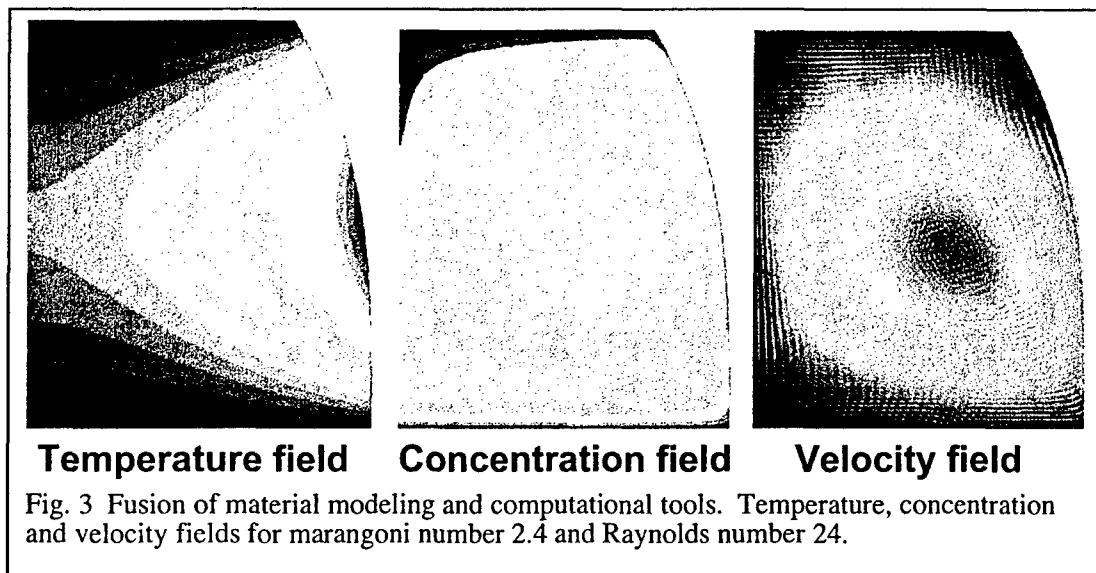$$x{=}0.25 \qquad\qquad x{=}0.4$$

Fig. 2 Chemistry of mullite

The performance of this class of materials depends directly on the quality of the crystals used, which, to a large extent, is determined by the uniformity of temperature and concentration at the growth interface during processing. Consequently, heat and mass transfer to and from the interface during growth, and their relationship to the thermal environment established by the furnace and the fluid flow in the melt, play key roles in controlling the solidification process. There has been a tremendous drive in the past decade to optimize and improve the conditions, configurations, and procedures for growing and processing crystals but there has been only a few experimental and modeling work for this family of materials. We investigated through

Temperature field   Concentration field   Velocity field

Fig. 3 Fusion of material modeling and computational tools. Temperature, concentration and velocity fields for marangoni number 2.4 and Raynolds number 24.

numerical modeling effort the solidification of $2Al_2O_3 \cdot SiO_2$ mullite, by the vertical Bridgman technique.

Status of Process Model: Combined Heat Transfer and Fluid Flow Analysis of Semi-Transparent Crystal Solidification -

The processing of the $2Al_2O_3 \cdot SiO_2$ mullite required temperatures of 2000 °C and greater and heat transfer at these very high temperatures are dominated by the radiation heat transfer mode. Yet, most of the numerical models developed for solidification of crystals have neglected the effects of radiation heat transfer within the crucible. Brown (1988) has made a comprehensive review of the papers. In general, these studies apply to solidification of semiconductors and cannot be generalized to represent the behavior of oxide crystals. The earliest investigations of the effect of radiation on nonopaque crystals is due to Viskanta and co-workers (Tarshis et al.; 1969 and O'Hara et al.; 1968, Viskanta; 1975). In these studies, the formidable general problem is reduced to a one-dimensional analysis of steady state conduction and radiation heat transfer as it occurs between two partially transparent media in intimate thermal contact. The models implemented in these works neglect many of the complexities of the actual growth process. Nevertheless, they show that the temperature distributions and the net thermal fluxes in a growing semi-transparent crystal are drastically modified by the participation of the media in the radiation transfer process. These investigations also conclude that radiative heat transfer stabilizes the interface. This occurs because the temperature gradients at the interface are steeper in combined radiative-conductive systems than for the purely conductive cases. This conclusion is later disputed by Abrams and Viskanta (1974). This finding is corroborated by two papers due to Antonov et al.(1980) and Yuferev and Vasil'ev (1987). These two investigations present a more realistic treatment of conduction and radiation heat transfer for growth of sapphire by the Stepanov's method. The analyses are still one-dimensional and still the radiation heat transfer can lead to instability in the crystallization front. It is also postulated that the pronounced stretching of the solid-liquid interface observed experimentally may be due to radiative transfer. Interaction of multi-dimensional radiation exchange with convection and

conduction was studied by Kassemi et al (1989, 1990) in the context of crystal growth by vapor transport. They used a finite difference control volume approach to discretize the diffusive and convective terms and an element-to-node zonal approach to represent the radiative exchange.

The results show that through interaction with convection radiation significantly affects the crystal shape. It was also shown that surface and internal radiation exchange have opposing effects on the interface curvature. The first studies to focus on solidification of semi-transparent oxides from melt in realistic crystal growth configuration have been due to Brandon and Derby (1991, 1992). Lin and Motakef (1993) considered solidification of BSO in a vertical Bridgman configuration. They solved the combined radiation conduction convection problem indirectly by iterating between the finite element code ABAQUS to solve the radiation-conduction problem in the solid and the fluids code FIDAP to solve the conduction-convection problem in the melt. In summary, the interactive effects of radiative heat transfer and convection on solidification of $YNbO_4$ and $2Al_2O_3 \cdot SiO_2$ will be investigated experimentally and isolated numerically in order to optimize the growth conditions for solidification of both materials.

DESIGN OF PROCESS MODEL

Physical Model: Mathematical Formulation

Oxide crystals have been usually grown by the Czochralski technique. In the Czochralski process, heat is supplied radially from the side to the crucible containing the charge and removed axially at the solidification front. This sets up an unsteady three-dimensional destabilizing buoyancy-driven convection that produces periodic fluctuations of the interface and generation of rotational impurities. Since the requirement for uniformity is more stringent for oxide crystals (with length scales on the order of centimeters) than for semiconductors, researchers have been forced to exploit other techniques for growing these materials. The vertical Bridgman and float zone techniques have been a favorite alternative and has been used for the investigation of $2Al_2O_3 \cdot SiO_2$ mullite solidification to reveal the intrinsic capabilities of these materials. In vertical Bridgman technique the crucible is aligned with the gravitational vector, convection in the melt is quite weak and the axisymmetric heat input and extraction from the sides results in a more stable axisymmetric solid-liquid interface.

A cross-sectional view of the cylindrical ampoule in a typical vertical Bridgman furnace configuration the ampoule which encapsulates both the solid and the melt is pulled downwards in the gravitational field through the temperature profile maintained along the bore of the furnace, at a constant velocity, U_{pull}. The three-zone furnace consisted of a hot section separated from the cold section by an insulated region. The temperatures in the hot and cold zones were maintained by the insulating walls, therefore, they werea assumed to be uniform at temperatures T_h and T_c, respectively. The insulated region was not actively controlled; thus, the temperature of the bore surface in this region varies linearly between the hot and cold ends. As a result the bore surface temperature can be assumed by the piecewise continuous profile. The boundary conditions has to be studied accurately for the $2Al_2O_3 \cdot SiO_2$ mullite crystals. The details of the geometry, temperature levels, and thermophysical and radiative properties are different for each crystal. Thus, the details of the thermophysical and radiative properties were investigated experimentally

and isolated numerically in order to optimize the growth conditions for solidification of both $2Al_2O_3 \cdot SiO_2$ mullite.

Radiation heat transfer

In solidification of semiconductors usually both the crystal and the melt are opaque to thermal radiation and both phases have relatively high thermal conductivities. Therefore, conduction is the dominant mode of heat transfer in both the solid and the melt. Oxide crystals, on the other hand, are usually semi-transparent to thermal radiation in the solid phase and almost opaque in the melt. They also have relatively low thermal conductivities in both phases. Therefore, heat transfer during the solidification of oxide crystal is governed by an intricate balance between convection and conduction in the melt and conduction and radiation in the solid. In a sense the solid acts basically like a light pipe through which the interface looses considerable amount of heat (by emission) to the cold sections of the crucible wall or directly to the furnace, if the crucible is also transparent. Therefore, radiation heat transfer plays dominant role in shaping the crystal interface. Through its interaction with natural convection, it can also drastically modify the flow fields in the melt and alter the segregation patterns at the growth front.

Governing Equations

The heat transfer mechanisms which govern solidification of oxides are complicated. There was a strong heat transfer link through radiation and natural convection between the furnace and the crucible. Consequently, the longitudinal temperature distribution of the bore surface was approximately imposed on the outer surface of the crucible. Heat transfer inside the crucible was dominated by conduction and convection in the opaque melt and by conduction and radiation through the semitransparent crystal. Therefore, at the inner crucible surface, in the melt region, there is a balance between the conductive fluxes. Similarly, at the inner crucible surface, in the crystal, there is a balance among the radial conductive fluxes through the ampoule and the crystal and the net radiative flux at the wall surface. Since the pulling velocity of the ampoule was small a quasi-steady approach was adopted and the negligible convective terms which arise due to the ampoule motion were not considered. The final location and shape of the interface (at quasi-steady-state) is of course determined by a balance among the conductive fluxes on both sides of the solidification front, the net radiative flux at the interface, and the released heat of fusion. For the materials considered here, and again due to the very slow pulling speed, the latent heat of fusion is negligible compared to the other terms in the energy balance but it is still retained in the interface equation for sake of completeness. Furthermore, since it was assumed that the longitudinal axis of the ampoule is aligned with the gravitational vector, the bore temperature profiles established by the furnace are circumferentially uniform and, therefore, axisymmetric conditions needs to be exploited. Following the quasi-steady approach, the energy equation describing heat transfer in the melt, the crystal and the ampoule is written as follows.

1. Crystal

$$\nabla^2 \theta + (Nr_s)\int_0^\infty (\nabla \cdot q_{r_\lambda})d\lambda = 0 \qquad \text{(EQ 1)}$$

2. Melt

$$\left(\Pr \frac{K_l}{K_s}(Gr)^{1/2}\right)\nabla \cdot \nabla\theta = \left(\frac{K_l}{K_s}\right)\nabla^2\theta \tag{EQ 2}$$

3. Ampoule

$$\nabla^2\theta = 0 \tag{EQ 3}$$

These equations are subject to the following thermal boundary conditions:

2. Melt-Ampoule Interface:

$$\left(\frac{K_l}{K_s}\right)\nabla\theta \cdot \hat{n}_{al} = \left(\frac{K_a}{K_s}\right)\left(\nabla\theta \cdot \hat{n}_{al}\right) \tag{EQ 4}$$

3. Crystal-Ampoule Interface:

$$-(\nabla\theta) \cdot \hat{n}_{as} = -\left(\frac{K_a}{K_s}\right)\left(\nabla\theta \cdot \hat{n}_{as}\right) - (Nr_s)\int_0^\infty\left(q_{a_\lambda} \cdot \hat{n}_{as}\right)d\lambda \tag{EQ 5}$$

3. Ampoule-Air-Furnace Interface:

$$-\left(\frac{K_a}{K_s}\right)\left(\nabla\theta \cdot \hat{n}_{a\infty}\right) = (Bi)(\theta - \theta_\infty) - \left(Nr_a\frac{K_a}{K_s}\right)\varepsilon_{a\infty}\left(\theta^4 - \theta_\infty^4\right) \tag{EQ 6}$$

4. Ampoule Top and Bottom:

$$\theta = \theta_c, \quad \theta_h \tag{EQ 7}$$

In addition to these boundary conditions, the energy equation is also subject to the following interface conditions.

$$\theta = \theta_m \tag{EQ 8}$$

and

$$-\left(\frac{K_l}{K_s}\right)(\nabla\theta) \cdot \hat{n}_{ls} = -\nabla\theta \cdot \hat{n}_{ls} - (Nr_s)\int_0^\infty\left(q_{s_\lambda} \cdot \hat{n}_{ls}\right)d\lambda - (St)(Pe) \tag{EQ 9}$$

An example of the proposed work can be examined using commercially available crystals of YAG and BSO and their radiative properties. The total divergence of radiative flux reduces to

$$\int_0^\infty\left(\nabla \cdot q_{r_\lambda}\right)d\lambda = 0 \tag{EQ 10}$$

The net radiative flux at the wall is given by

$$\int_0^\infty \left(q_{a_\lambda} \cdot \hat{n}_{as}\right) d\lambda = \varepsilon_{as} F_{0-\lambda_c}(\lambda_c, \ T_a)\theta_a^4$$

$$-\int_{A_a} \varepsilon_{as} F_{0-\lambda_c}(\lambda_c, \ T_a)\theta_a^4(r') \overline{WW}(r', \ r)dA \qquad \text{(EQ 11)}$$

$$-\int_{A_s} \varepsilon_{ls} F_{0-\lambda_c}(\lambda_c, \ T_m)\theta_m^4(r') \overline{SW}(r', \ r)dA$$

Similarly, the net radiative flux at the interface is given by

$$\int_0^\infty \left(q_{a_\lambda} \cdot \hat{n}_{ls}\right) d\lambda = \varepsilon_s F_{0-\lambda_c}(\lambda_c, \ T_m)\theta_m^4$$

$$-\int_{A_a} \varepsilon_{as} F_{0-\lambda_c}(\lambda_c, \ T_a)\theta_a^4(r') \overline{WS}(r', \ r)dA \qquad \text{(EQ 12)}$$

$$-\int_{A_s} \varepsilon_s F_{0-\lambda_c}(\lambda_c, \ T_m)\theta_m^4(r') \overline{SS}(r', \ r)dA$$

The challenge for the $2Al_2O_3 \cdot SiO_2$ mullite investigation was the quantitative determination of Equations 1 through 10 in a form suitable for inclusion $2Al_2O_3 \cdot SiO_2$.

The fluid flow in the melt which is primarily driven by the buoyancy force is described by the continuity and balance of momentum equation and is subject to non-slip boundary conditions at all solid boundaries.

1. Continuity:

$$\nabla \cdot \vec{V} = 0 \qquad \text{(EQ 13)}$$

2. Momentum:

$$\left(Gr^{1/2}\right)\vec{V} \cdot \nabla\vec{V} = -\nabla P + \nabla^2\vec{V}\left(Gr^{1/2}\right)(\theta - \theta_m) \qquad \text{(EQ 14)}$$

3. Non-Slip Boundary Condition:

$$\vec{V} = 0 \qquad \text{(EQ 15)}$$

Finally, these equations are subject to symmetry conditions along the centerline of the ampoule:

$$\vec{V} \cdot \hat{n}_r = 0$$

$$\vec{V} \cdot \hat{n}_z = 0 \qquad \text{(EQ 16)}$$

In writing the above equations its was also inherently assumed that the thermophysical properties of the solid and the melt although different are constant throughout each phase, the gap between the furnace bore and the crucible wall is small so that the external radiation exchange between elements on these two surfaces is basically one to one (view factor is one), and all surfaces in the model are treated as diffuse for the radiation exchange calculations. For

the solidification processes which involve doping, the species transport equations and their associated boundary conditions which include solutal rejection at the growth interface will be formulated and incorporated in the numerical model. Solution of the final system of integro-partial differential equations will describe the dynamic coupling and temporal link between the species, fluid flow temperature and radiation fields.

Numerical Formulation and Results

The finite element code FIDAP was adopted to solve the solidification problem. FIDAP has to be modified significantly in order to incorporate a radiative heat transfer model based on an exchange factor scheme, similar to the DEF method described by Naraghi and Kassemi (1989) into the code. The diffusive and convective terms in the governing differential equations were discretized based on the regular Galerkin formulation. Discretization of the integral terms describing radiation exchange using the exchange factor method were necessary to achieve a set of algebraic equations which can be incorporated in both finite element and finite difference codes. The exchange factor methods have been already used with both finite element and finite difference techniques and have produced very accurate results (Kassemi and Naraghi 1993, Saltiel and Naraghi, 1990). Nine-node quadratic continuum elements and three-node quadratic surface elements was used throughout the mesh. The radiation flux terms can then be evaluated at these integration points.

The resulting set of discretized algebraic equations will be solved using a segregated approach which tackles every single degree of freedom individually (Engleman, 1993). That is, the solution matrix is decomposed into smaller loosely connected sub-matrices each associated with only one conservation equation. The smaller matrices are then solved in a sequential manner using gaussian elimination. Because these matrices are loosely connected the method has a slower convergence rate compared to the coupled direct solvers. However, the scheme is fairly robust because it has a large radius of convergence and does not require a good starting guess. The degrees of freedom are decoupled, it is much less demanding with regard to computer storage needs as compared to coupled solvers.

The solidification of mullite was treated by tracking the interface as a free surface. In contrast to the coupled solvers where the new interface position is part of the solution vector, in the segregated approach an iterative scheme is adopted. First, the conservation equations are solved assuming a fixed interface location and using the continuity of temperature at the interface (Eq. 11) as a boundary condition to the energy equation. Next, the required change in the interface location is determined by satisfying the interface energy balance condition (Eq. 12). The updated interface position is then used again to solve the conservation equations. This iterative process is continued until a converged solution is attained. During each simulation, as the solidification front moves and changes shape, the interface position is tracked and the position of the nodes are changed along straight lines (spines) in proportion to the movement of the interfacial nodes.
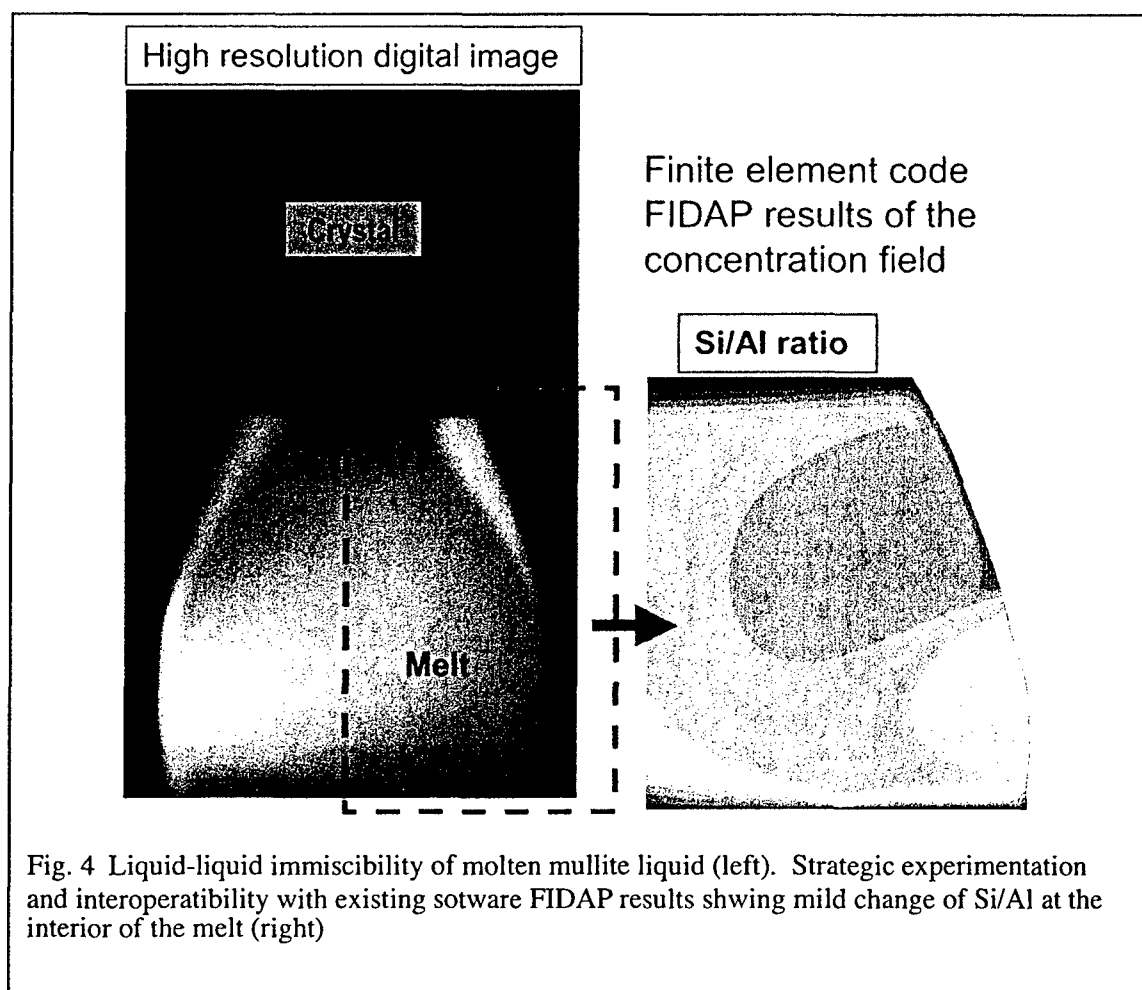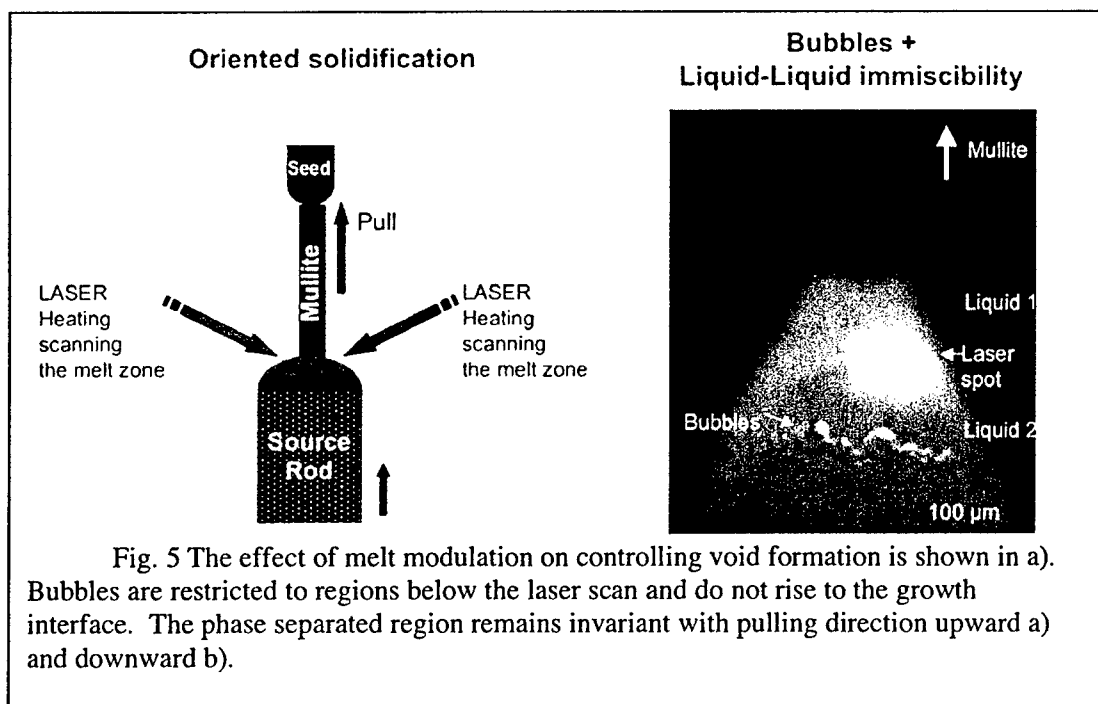
Fig. 4 Liquid-liquid immiscibility of molten mullite liquid (left). Strategic experimentation and interoperatibility with existing sotware FIDAP results shwing mild change of Si/Al at the interior of the melt (right)

The results for the temperature- concentration- and velocity field are shown in Fig. 3 for dimensionless Marangoni number 2.4 and dimensionless Raynolds number 24. Figure 3 is results for the large diameter solidification condition. The fundamental challenge the coupling between temperature and velocity field to produce concentration field. As will be discussed further in following section single crystal growth of $2Al_2O_3 \bullet SiO_2$ mullite was preceded with liquid-liquid immiscibility. The high-resolution digital images of laser heated float zone system revealed that the melt separated into two immiscible liquid as determined from the different optical transmission characteristic, Fig. 4. Finite element code FIDAP results also included in Fig. 4 and reveals mild change of Si/Al ratio in the molten liquid. The molten zone of the growth experiments with the $3Al_2O_3 \bullet 2SiO_2$ mullite compositions were quenched to analyze global chemical partitioning in the melt. The experimental results could not identify in significant compositional differences the length scales of molten zone within the range 40 to 600 μm. Finite element code FIDAP results showed spatial change in the Si/Al ratio. Although this change was very small, it was suffient to have different degree of polymerization of tetrahedral connectivity of the molten $Al_2O_3 \bullet SiO_2$ composition. This had tremendous effect on the viscosity of the melt and by far most important parameter was the temperature of the melt to alter the

degree of the polymerization. In fact, to fabricate single crystal $2Al_2O_3 \cdot SiO_2$ mullite, melt had to be heated at temperatures exceeding 2100 °C. This means at least 200 °C superheating to produce single crystals. The starting composition $3Al_2O_3 \cdot 2SiO_2$ mullite could be melted at temperature 1800 °C and wide range microstructures could be produced at temperature region between 1800 to 2200 °C.

Growth Experiments

The crystal growthinvestigation was initiated to determine in more detail the growth behavior of mullite single crystal fibers. The primary objective of this work was to determine the growth characteristics of single crystal mullite fibers grown by the Laser Heated Floating Zone-Method (LHFZ) and compare the results with fibers grown by Edge-Defined Film Fed Growth (EFG). The effect of different supercooling conditions and starting compositions were compared. Also included in this study are the effects of melt modulation to minimize void formation. Another objective was to study the tensile failure of mullite fibers. The results and possible mechanisms are discussed by examining the relationships between growth characteristics, fracture stress, and mullite fiber microstructures. The growth characteristic of fibers in the SiO_2-Al_2O_3 system has not been documented and findings presented here provide a valuable supplement to understanding the tensile strength characteristics of mullite filaments.

Fig. 5 The effect of melt modulation on controlling void formation is shown in a). Bubbles are restricted to regions below the laser scan and do not rise to the growth interface. The phase separated region remains invariant with pulling direction upward a) and downward b).

There are at least two major sources of heterogeneities in aluminosilicate melts during laser heated float zone growth. The first heterogeneity is the development of gas bubbles and the

second is liquid-liquid immiscibility. These heterogeneties have profound effects on the fiber growth process and resulting mechanical and microstructural fiber characteristics. The effect of bubbles in the high viscosity SiO_2-Al_2O_3 melt on fiber growth can be minimized by a melt modulation technique, a new heating technique which eliminates bubbles from the growth front region. The SiO_2-Al_2O_3 melt has high a viscosity and is known to entrap bubbles coming from the source materials. The bubbles can be entrapped in the fiber as voids (flaws) and can either be present on the surface or in the bulk of the material. The dynamic nature of the molten zone and bubble formation or removal was monitored *in situ* from high-resolution digital images. Melt modulation effectively eliminated void formation at or near the surface of solidifying fibers. Figure 6 shows a photograph of a mullite fiber grown with the melt modulation technique in which the transverse scan-length was larger than the molten zone diameter. This technique agitates the molten liquid of SiO_2-Al_2O_3. There was no indication of bubble formation above the laser scanning plane during growth. The absence of voids was confirmed by subsequent SEM and TEM examination. Fibers, with very few exceptions, fractured from surface flaws. The growth of void free fibers at high pull-rates was not possible with stationary heating. The dominant feature of stationary laser heating is that a large amount of energy is absorbed in a small area in a short time and, hence, does not eliminate the void formation as effectively as the scanning technique. The melt-modulation technique has at least two additional advantages. First, a more uniform temperature distribution can be achieved in the molten zone. Uniform growth temperature is a prerequisite for any crystal growth system and it is even more important for the growth of mullite single crystals which show a strong tendency for facet formation (Fig. 7). Second, mixing in the melt can be improved by vibration of the melt with different scan frequencies.
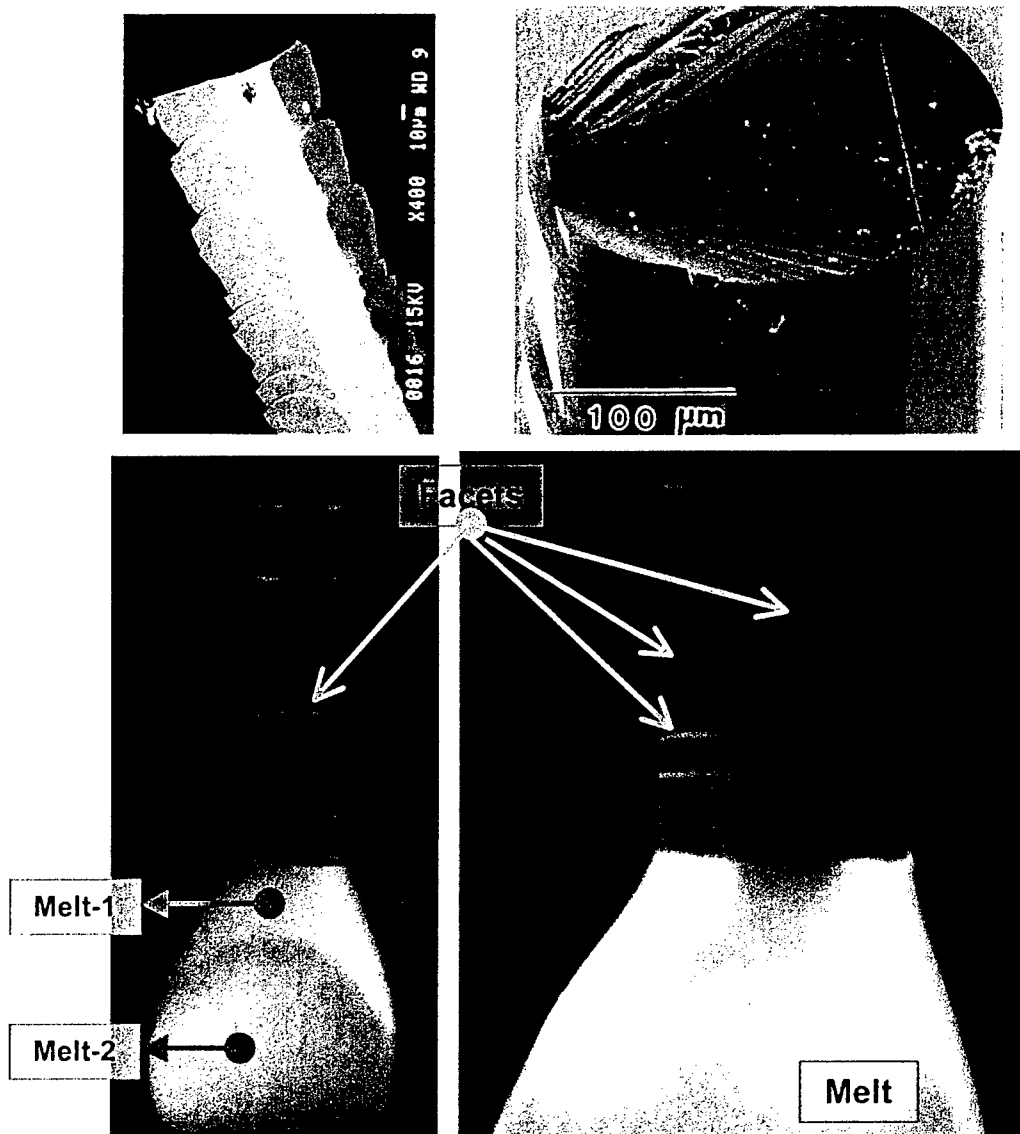
Fig. 6 Complex coupling between different transport mechanism at the interface. High resolution digital images showing faceted growth.

The second major source of heterogeneities in SiO_2-Al_2O_3 melts, liquid-liquid immiscibility in the high Al_2O_3 compositions, has been suspected, but so far has not been unambiguously demonstrated. The review of stored images revealed that liquid adjacent to single crystal mullite crystals was more transparent than in the interior of the melt (Figs. 1, 2, and 3). The position of the darker dome shaped interior liquid was not effected by the laser impingement position. Reflected optical microscopy of longitudinal cross-sections of quenched molten zone specimens showed scattering intensity features that correspond with the images shown in Figs. 1 and 2.

Hence, we interpreted these features arising from an immiscibility in the liquid, possibly due to compositional and/or structural differences in the melt.

Usually systems with a miscibility gap in the liquid phase have density differences between the two liquid phases large enough for the two phases to remain separated as long as they are kept above the monotectic temperature,T^M, and below the convolution temperature T^C. However, the anticipated density differences in the SiO_2-Al_2O_3 system are not expected to be large enough to form separate layers. The tendency for layer separation was examined by comparing upward and downward growth conditions. The spatial position of the darker area was invariant with respect to growth direction (Fig.6) and remained attached to the source rod. The density differences in the two immiscible regions, therefore, are insignificant. Yet, there was apparently enough difference in surface tension between the two liquid phases to form separate regions in the molten zone. Similar immiscibility regions were observed for all compositions studied.
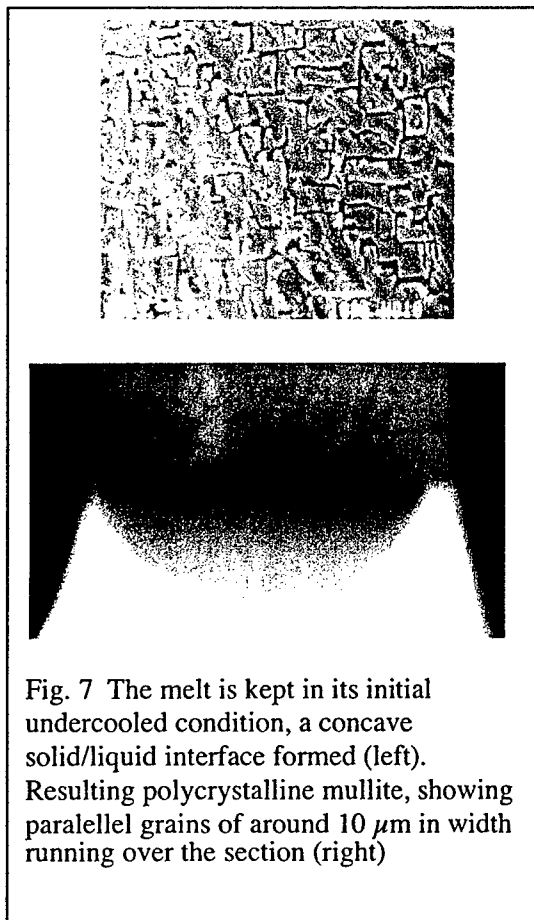

Fig. 7 The melt is kept in its initial undercooled condition, a concave solid/liquid interface formed (left). Resulting polycrystalline mullite, showing paralellel grains of around 10 μm in width running over the section (right)

The immiscibility of SiO_2-Al_2O_3 in this composition range was first suggested by Aramaki and Roy in a study in which they stated that, on the basis of Dietzel's field strength[29] calculations, a wide (60 mole % Al_2O_3 ; 3:2 mullite) miscibility gap might be expected at temperatures below 2000 °C. Galakhov and Konolova, and McDowell and Beall also suggested possible liquid phase separation. Recently Rishbud's, Rishbud and Pask's and Kuo's calculations using mullite
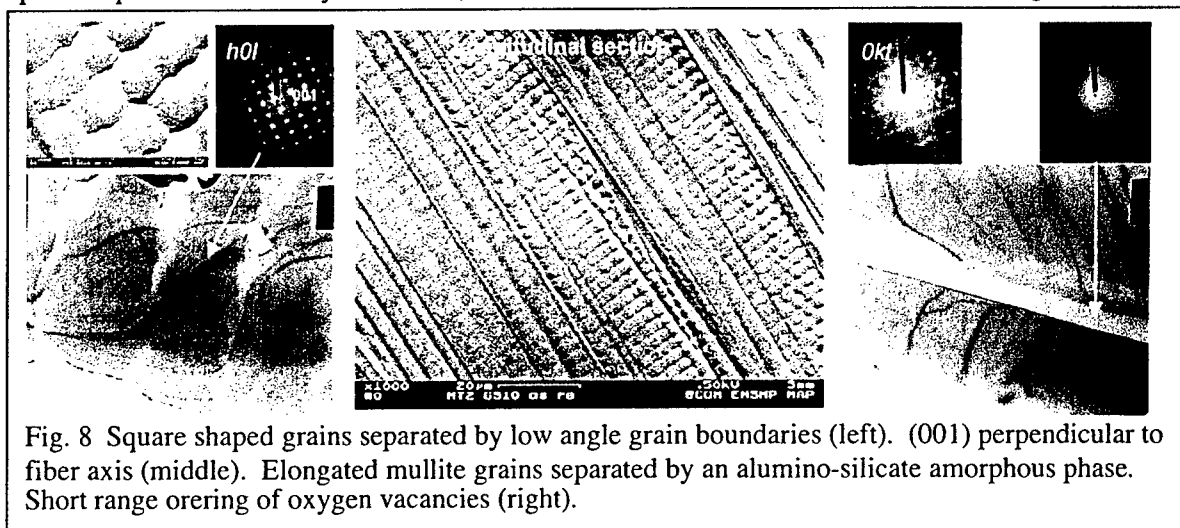

Fig. 8 Square shaped grains separated by low angle grain boundaries (left). (001) perpendicular to fiber axis (middle). Elongated mullite grains separated by an alumino-silicate amorphous phase. Short range orering of oxygen vacancies (right).

and alumina as chemical species in the solution model predicted stable liquid immiscibility at temperatures up to and greater than 2100 °C. However, a miscibility gap in the SiO_2-Al_2O_3 system at high Al_2O_3 concentrations and at $T > T^M$ has not been experimentally observed. The liquid-liquid miscibility gap observations presented here provide the first experimental evidence for liquid immiscibility for these compositions and temperatures. Our experimental observations suggest that liquid immiscibility remains a dominant heterogeneity in the molten zone during crystal growth at steady-state conditions even for higher temperatures.

Fibers grew as single crystal or polycrystalline mullite as a function of the growth conditions and seeding. The polycrystalline fibers can be grown from all compositions studied in the present work at steady-state conditions as long as the melt stays in its initial undercooled condition, Fig. 7. The SEM and TEM analysis revealed that polycrystalline fibers consist of highly elongated and faceted mullite crystals bounded by aluminosilicate glass (Figs. 8). Fiber cross sections are quite round and faceting along the fiber length is absent. The absence of alumina in these fibers was confirmed by X-RAY and TEM characterization. These results and the microstructure shown in Figs. 8 are similar to those observed by Aksay and Pask and Kriven and Pask[20] on rapidly cooled mullite. Their interpretation of the microstructures on the basis of the supercooling of the liquid is in agreement with our observations.

The mullite fibers studied are transparent, their cross sections are not circular but facetted with dimension of 100 to 150 μm. They can enclose very fine silica rich intergranular phases as shown by electron microprobe analysis (EPMA-WDX) separating elongated grains. These grains have an Al/Si atomic ratio of ~4.4 which corresponds to x~0.45 (Al/Si = (4+2x)/(2-2x). The growth direction corresponds to [001].
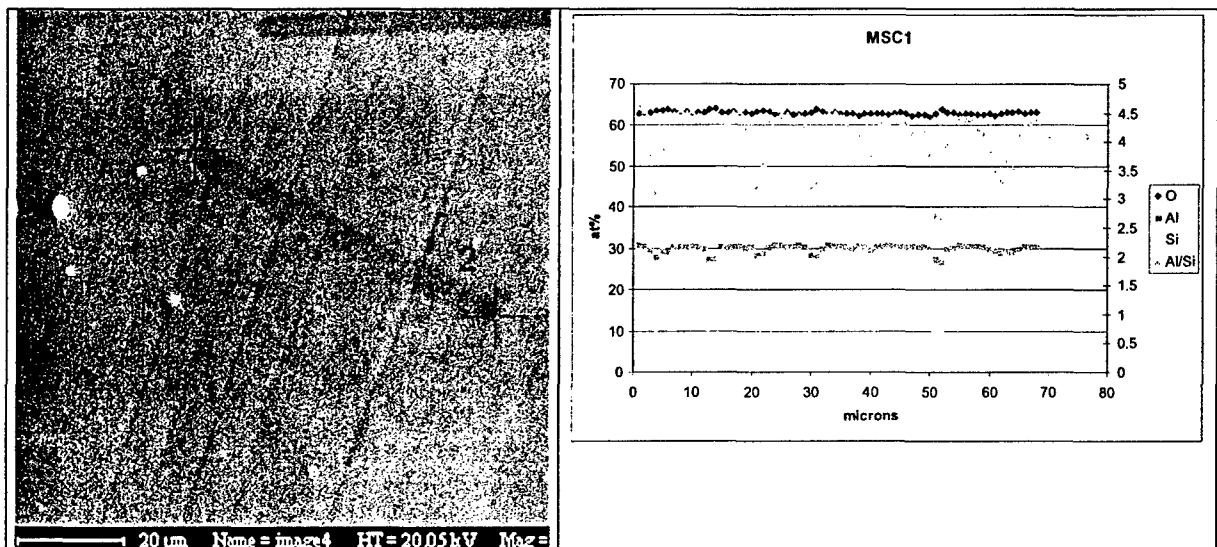

Fig. 9 WDX profile

The liquid-liquid immiscibility and its consequences on single crystal growth can be deduced by the observation of seeding and subsequent single crystal growth of mullite. Fig.7

Composition	a, [nm]	b, [nm]	c, [nm]
M70.4(2)	0.7586	0.7684	0.2885
M71.0(2)	0.7589	0.7681	0.2888
M72.0(2)	0.7589	0.7690	0.2899

Table 1 The lattice parameters for M70.4(2), M71(2) and M72(2) materials were calculated from x-ray diffractometry scans.

Is a representative of single crystal mullite growth using polycrystalline seed material. As growth initiates, Fig. 6, the fibers are polycrystalline and the liquid/solid interface is macroscopically very rough (Fig. 3a). By increasing the melt temperature, a planar/liquid-solid interface, can be established as shown in Fig. 6. Thus single crystal growth can been achieved by establishing steady-state growth conditions from a polycrystalline fiber interface (Fig. 5 and 7). Although the exact values are yet not known for T^M and T^C, the planar growth interface in the present work was attained below T^C, for all compositions studied. Thus single crystal growth was achieved without a complete monotectic invariant transition in the liquid state. This suggests that the faster diffusion rates obtained by increasing temperature to achieve planar growth overcome the constitutional supercooling.

The lattice parameter differences measured over the narrow composition range followed the reported trend of **a** and **c** increasing with alumina content (Table 1). However the **b** parameter did not consistently decrease as has been reported. The differences were not statistically significant. Both lattice parameter values and ordering values fall within the reported range for material compositions more alumina rich than 2:1 but clearly lower than 5:2. As observed in TEM, mullite single crystals are free of dislocations, low angle boundaries and voids. Single crystal mullite showed a high degree of oxygen vacancy ordering (x = 0.47, both **e** and **f** reflections present, Cameron). Single crystal growth can also be achieved by changing the modulation frequency (scan-velocity) of the laser heating. The degree of supercooling diminishes as the solution agitation is increased. These observations lead us to suggest that formation of mullite in aluminosilicate melts is, in fact, preceded by immiscibility. Thus, the mullite growth is accompanied by formation of a stagnant SiO_2-rich liquid layer at the solidifying interface.

Figure 6 also demonstrate facet formation in single crystal mullite fibers. The crystallographically induced metastability manifests itself, as a preferential growth of specific planes. This continued until sufficient departure from the equilibrium concentration developed and was followed by sudden transversing the solidifying interface direction. This formed a "bamboo" type fiber as shown in Figs. 7. This was accompanied by a change between the equilibrium contact angle, between the facet face and the rest of the interface (Fig.7) such that fiber growth was not centrosymmetric with respect to the fiber axis and molten zone. The selective adsorption in the solution causes a decrease of the surface free energy of fast growing plane and the wetting angle. The deviation of the wetting angle with respect to average surface energy of the fiber liquid system is depicted clearly in Figs. 6. The growth of high strength fibers requires tight control of "surface tension balance " at the point of intersection of the interface. Bolling and Tiller showed that this depends on the temperature gradient, surface tension, and the entropy of fusion per unit volume for a pure material. This implies that in a

heterogeneous liquid phase in which the activity of each component varies with concentration, the faceting tendency will be further complicated by mixing free energy. This suggests the necessity to study the orientation relationship between supercooling and preferred growth direction of mullite single crystals. SEM analysis revealed that the fibers were indeed strongly faceted (Fig. 6) and typically exhibit two large flat surfaces (presumably {110}) about the circumference. The cross-sectional shape can become highly oblate as the facet size increases. Faceting also occurs along the fiber length causing sharp changes in fiber diameter (bamboo type fiber).

Mullite structure

Mullite is a solid solution of Al_2O_3 and SiO_2 the chemical formula of which can be written as $Al^{VI}_2(Al^{IV}_{2+2x}Si^{IV}_{2-2x})O_{10-x}$. The mullite structure is obtained from the silimanite one (x=0, $Al_2O_3 \cdot SiO_2$) by the substitution of Si^{4+} by Al^{3+} cations. This substitution is counterbalanced by the creation of oxygen vacancies $2Si^{4+} + O^{2-} \rightarrow 2Al^{3+} + \square$. The molar ratio $3Al_2O_3 \cdot 2SiO_2$ or x=0.25 corresponds to the stable form of mullite (also called "stoichiometric mullite"). However the low interdiffusion rates of aluminum and silicon through the mullite crystal make the synthesis of metastable compounds $Al^{VI}_2(Al^{IV}_{2+2x}Si^{IV}_{2-2x})O_{10-x}$ possible, with a large range of x. Composition from around x=0.25 ($3Al_2O_3 \cdot 2SiO_2$) up to x=0.8 have been reported. The synthesis route (i.e. solidified from the melt, obtained by solid state sintering from ceramic powders or sol precursors mixed at the atomic or nanometer scales), the rate of cooling, the presence or absence of α-Al_2O_3 seeds, and the degree of silica evaporation are some of the experimental factors explaining the differences in the compositions and structures reported in the literature. They have in turn a direct influence on the structural and functional properties of mullites. As an example, the ordering processes of the oxygen vacancies have been pointed out as a key factor to understand the remarkable thermo-mechanical stability of mullite.

The structure of mullite is derived from that of silimanite (x=0, $Al_2O_3 \cdot SiO_2$) in which AlO_6 octahedral chains sharing edges run parallel to the c-axis and are cross-linked by doublets of SiO_4 and AlO_4 tetrahedra. In the silimanite, Al and Si atoms are completely ordered in the tetrahedral chains with a unit length a~7.6Å, b~7.7Å, c~5.8Å. The mullite structure is obtained from the silimanite one by the substitution of Si^{4+} by Al^{3+} cations. This substitution leads to an apparent long range disorder of Al and Si cations in the tetrahedral sites. As a result the c-dimension for the average structure becomes half that of the silimanite. The cation substitution in the tetrahedra is counterbalanced by the creation of oxygen vacancies $2Si^{4+} + O^{2-} \rightarrow 2Al^{3+} + \square$. Moreover the two cations which have lost bridging oxygen atoms are coordinate to only three oxygen atoms, and therefore are displaced from the T site to a new position $^{IV}Al^*$. The adjacent O_c site is displaced off the symmetry center toward the $^{IV}Al^*$ site to a new Oc^* site and is now three coordinated by tetrahedral cations.

With the assumption that the vacancies are randomly distributed in the structure, mullite is described by an average structure presented in Table I.
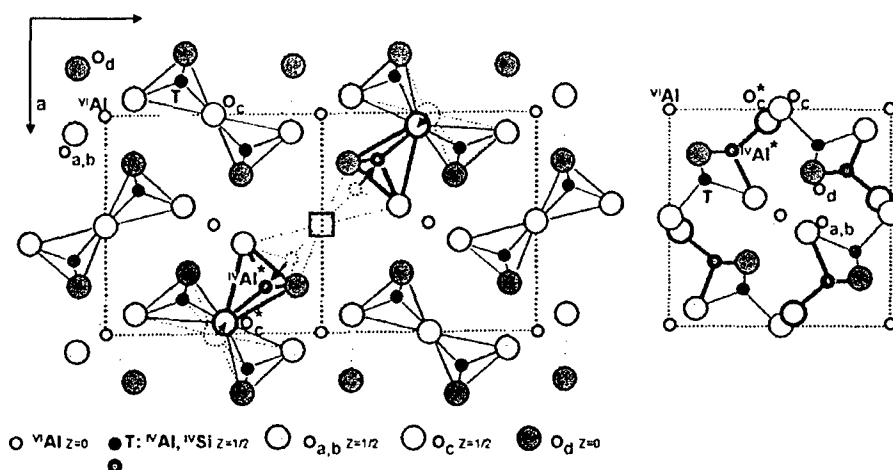
Fig. 10 Atomic displacements around oxygen vacancy in mullite, average structure.

Site	Al^{VI}	T	^{IV}Al*	O$_{a,b}$	O$_d$	O$_c$	Oc*
Position	0 0 0	~0.15, ~0.34 0.5	~0.26 ~0.21 0.5	~0.36 ~0.42 0.5	~0.13 ~0.22 0.5	0.5 0 0.5	~0.44 ~0.05 0.5
Occupancy	1	Al : 0.5 Si : 0.5-y	y	1	1	1-3y	y
Number of site per unit cell	2	4	4	4	4	2	4
number of atoms per unit cell (2y=x)	2	Al : 2 Si : 2-4y	4y	4	4	2-6y	4y

The stable form of mullite, also called "stoichiometric" mullite corresponds to x=0.25 (or $3Al_2O_3 \cdot 2SiO_2$).

Oxygen vacancy ordering in alumina rich mullites

Mullites show in the reciprocal space a complex scheme of sharp and diffuse satellite reflections and diffuse streaks, in addition to the Bragg reflections expected from the Pbam space group, Fig. 10. They reveal a non random distribution of the oxygen vacancy. These additional reflections change their sharpness and position according to the alumina content and preparation mode. Structural models have been proposed in the literature to explain the various diffraction patterns obtained, they correspond either to long range ordering or short range ordering of the vacancies.

Sharp satellite reflections are associated to a long range order of the vacancies. There are visible for SAD pattern in the [010] zone axis. Alumina rich mullites (x≥0.4, 2:1 molar ratio) show in the reciprocal space Various structural models are proposed in the literature to explain these

diffraction patterns. Nakajima et al[1]. report a high degree of order in the oxygen vacancy arrangement. The diffraction patterns and the HREM images of alumina rich mullites are induced by an incommensurate modulation of the structure with the formation of ordered domains exhibiting antiphase relations parallel to the c-axis, and an incommensurate period along the a-axis. In opposition to this description, Rahman propose that these diffraction patterns are caused by a short-range ordering of the oxygen vacancies. The structure is then described via inter-vacancy correlation vectors, the sequence and frequency of which depend on the alumina content, Fig. 11.

Investigation of images taken around Scherzer defocus with a zone axis [3$\underline{1}$0] in a rather thick zone showed that the corresponding FFT had extra spots at $\pm h/3$, $\pm k$, $\pm 1/2$ and diffuse streaks around these spots parallel to [001]*, as in a SAD pattern. The HR image shows variations in intensity of the dots, Rhaman have attributed these variations to variations in vacancy concentration along the incident beam. Their image simulations for similar conditions of defocus show that highest concentrations give brightest spots. The binary image has been derived by a thresholding on the gray level, to select the brightest dots (last class of the histogram, 2800-3200). These dots are distributed preferentially along specific directions as [131] and [261], rows pointed by the arrows. However this directions of alignment do not contribute to the contrast enhancement around $\pm h/3$, $\pm k$, $\pm 1/2$, seen on the FFT of threshold image, and already described for the SAD patterns. In order to evidence the origin of this periodicity on the vacancy distribution, an inverse FFT images built from respectively the spots a and a', has been superimposed to the corresponding threshold image. The resulting image reveals domains of a few nanometers in which the vacancies tend to form to form a superlattice, Fig. 12.

From this first analysis it can be concluded that disparities in the vacancy distribution along [3$\underline{1}$0] in the O_C columns are seen. The vacancy rich columns tend in turn to form ordered domains with super lattice dimensions (planes $\pm 1/3$, $\pm 1,1/2$ and $\pm 2/3$, $\pm 2,1/2$). In addition rows of several vacancies rich columns are frequently seen along [131] an [261]. The domains of oxygen vacancy ordering is shown in Fig. 12.
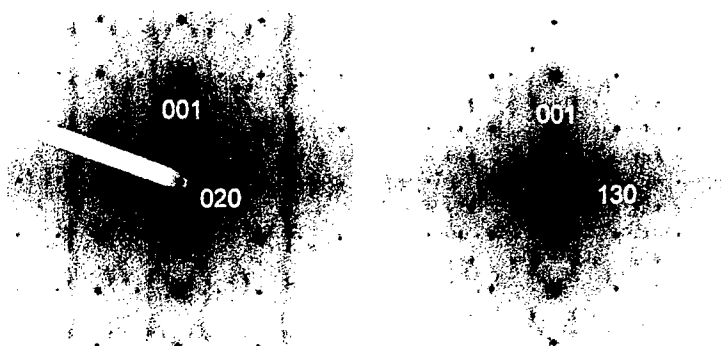

Fig. 11 Extra reflections has been due to a short range ordering of oxygen vacancies which are characterized in terms of distribution frequency of intervacancy vectors.

[1] Y. Nakajima et al. American Mineralogist **66** (1981) 142-147
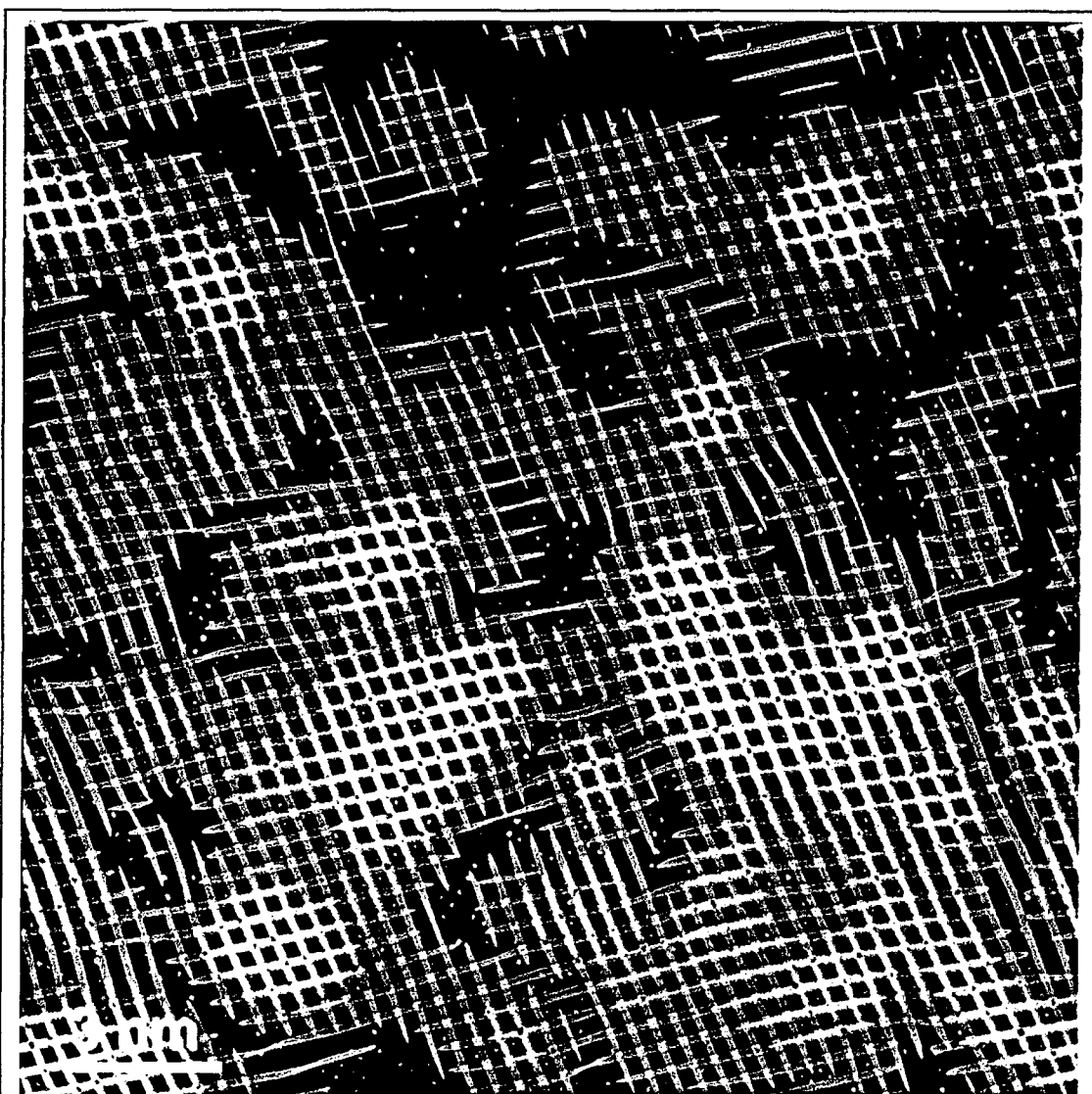
Fig. 12 Oxygen vacancy ordering in mullite as revealed first time.

CONCLUSIONS

Directionally solidified fibers with nominal mullite compositions of $3Al_2O_3 \cdot 2SiO_2$ were grown by the laser heated float zone (LHFZ) method. High resolution digital images from an optical microscope evidence the formation of a liquid-liquid miscibility gap during crystal growth. Experimental evidence shows that the formation of mullite in aluminosilicate melts is in fact preceded by liquid immiscibility. SEM analysis revealed that the fibers were strongly faceted and that the facets act as critical flaws. Examined in TEM, these mullite single crystals are free of dislocations, low angle boundaries and voids. Single crystal mullite showed a high degree of oxygen vacancy ordering. Regardless of the starting composition, the degree of order observed in polycrystalline fibers was lower than that observed in the mullite single crystals. Mullite formation (stable or metastable crystalline phases, polycrystalline or single crystal) is a function of the melt temperature. Formation of a stagnant liquid layer and phase separation is strongly dependent on the diffusional properties of the liquid and directly affects the type of crystal grown.

It was proposed that the growth of single crystal mullite is controlled by kinetics and thus it is a non-equilibrium process. Liquid-liquid immiscibility and slow diffusion rate of cations did not permit the growth of 3:2 mullite single crystals. Mullite exhibits remarkable thermomechanical stability. Crystals grown from the melt show a higher degree of oxygen vacancy ordering and resisance to dislocation motion. Columns of O_c tend to forma ordered domains with superlattice dimensions (planes $\pm 1/3$, ± 1. ½ and $\pm 2/3$, ± 2, ½). Vacancy rich colums are frequently seen along [131] and [261]. Further refined simulations using supercell to describe the periodicity of vacancies is required.

REFERENCES

Abrams, M. and Viskanta R., 1974, The Effects of Radiative Heat Transfer Upon Melting and Solidification of SemiTransparent Crystals, *J. of Heat Transfer*, Vol, p.184.

Al-Assafi, Cruse, A. T., Simmons, J. H. , Brennan, A. B. and Sacks, M. D. (unpublished work).

Aksay, A., Dabbs, , D. M. and Sarikaya, M. , J. Am. Ceram. Soc., 74 [10] 2343 (1991).

Aramaki, S. and Roy R. ,J. Am. Ceram. Soc., 45 [5] 229 (1962).

Aksay, I. A. and J. A. Pask, Science, 183 [4120] 69 (1974)

Aksay, I. A., and J. A. Pask, J. Am. Ceram. Soc., 58 [12] 507 (1975).

Anisimov, Y. S. , Grits E. F. and Mitin, B. S. Inorganic Mat, 13 [8] 1444 (1977).

Aizu, K., Possible Species of Ferroelastic Crytals and of Simultaneously Ferroelectric and Ferroelastic Crystals, *J. Phys. Soc. Japan,* Vol. 27, p 387 (1969).

Aramaki, S. and Roy, R. J. Am. Ceram. Soc., 43 [8] 670 (1960).

Aizu, K., Possible Species of Ferromagnetic, Ferroelectric and Ferroelastic Crystals, *Phys. Rev., B2* p 754 (1970).

Antonov, P.I., Bakholdin, S.I., Tropp, E.A, and Yuferev, V.S., 1980, An Experimental and Theoretical Study of Temperature Distribution in Sapphire Crystals Grown from the Melt by Stepanov's Method, *J. Crystal Growth*, Vol. 50, p.62.

Bailey, J. E., Monoclinic - Tetragonal Transformation and Associated Twinning in Thin Films of Zirconia, *Proc. Roy. Soc.* Vol. A 279 [1378] p. 395 (1964).

Boulesteix, C., Caro, P. E., Loier, Ch. and Portier, R., Determination of Twinning Elements for Mechanical Twins in the Rare-Earth Sesquioxides of Monoclinic Structure, [in French], *Phys. Stat. Solidi* A Vol. 11 p.771 (1972).

Becher, P. F. ,J. Am. Ceram. Soc., 74 [2] 255 (1991).

Bowen, N. L. , and Greig, J. W. , J. Am. Ceram. Soc., 7 [4] 238 (1924).

Bauer, W. H. , Gordon, I. , and Moore, C. H. , J. Am. Ceram. Soc., 33 [4] 140 (1950).

Brown, R. A. , AIChE Journal, 34 [6] 881 (1988).

Bolling, G. F. , and Tiller, W. A. , J. Appl. Phys., 31, 1345 (1960).

Bolling, G. F. , and Tiller, W. A. , J. Appl. Phys., 31, 2040 (1960).

Boulesteix, and P. E., Loier, Ch., Electron Microscopy Study of the Interpretation of Mechanical Twinning in crystalline Thin Films - Role of Microtwinning, [in French], *Phys. Stat. Solidi A,* Vol. 18, p.553 (1973).

Bowles J. S., and Mackenzie, J. K., The Crystallography of Martensite Transformations, I. Acta Met., Vol. 2, p. 129, (1954).

Mackenzie, J. K. and Bowles, J. S., The Crystallography of Martensite Transformations, II. Acta Met., Vol. 2, p. 138, (1954).

Bowles J. S., and Mackenzie, J. K., The Crystallography of Martensite Transformations, III. Face-Centered Cubic to Body-Centered Tetragonal Transformations, Acta Met., Vol. 2, p. 129, (1954).

Bilby, B. A. and Christian, J. W., Martensitic Transformations. Institute of Metals Mongr. and Report Series, No. 18, p. 121 (1955).

Brandon, S., and Derby, J.J., 1991, *J. Crystal Growth*, Vol. 110, pp. 481.

Brandon, S., and Derby, J.J. 1992, Heat Transfer in Vertical Bridgman Growth of Oxides: Effects of Conduction, Convection, and Internal Radiation, *J. Crystal Growth*, Vol. 121, p. 473.

Buerger, M. J., Polymorphism and Phase Transformations, *Fortschr.Miner.* Vol.39, p.9.

Cahn, R. W., Twinned Crystals, *Advances in Physics*, Vol. 3 [12] p. 363 (1954).

Chan, C. J., Lange, F. F. F., Rühle, M., Jue, J. F. and Virkar, A. V., Ferroelastic Domain Switching in Tetragonal Zirconia Single Crystals - Microstructural Aspects, *J. Am. Ceram. Soc.* Vol. 74 [4] p.807 (1991).

Christian, J. W., *Inst. Met. Monogr.* No. 33 p. 129 (1968).

Christian, J. W., Applications of the Phenomenological Theories of Martensite. Parts I. & II., *J. Inst. Met.* Vol. 84 p.386 (1955).

Clapp, P. C., A Localized Soft Mode Theory for Martensitic Transformations, *Phys. Stat. Solidi B,* vol. 57 p 561 (1973).

Claussen, N., Rühle, M. and Heuer, A. H. , Eds. Science and Technology of Zirconia II in *Advances in Ceramics*, vol. 12. Publ. by the American Ceramic Society, Columbus, Oh, USA (1984).

Cockayne, B., Chesswas, M., and Gasson D.B., Facetting and Optical Perfection in Czochralski Grown Garnets and Ruby, J. Mat. Science, Vol. 4, p. 450.

Cohen, M., Olson, G. B. and Clapp, P. C., On the Classification of Displacive Transformations, *Proc. Int. Cong. On Martensitic Transformations (ICOMAT), 1979*; MIT, Cambridge, MA, USA, pp 1-12 (1980).

Cox, D.E., High-resolution Powder Diffraction and Structure Determination, in Chap. 9 "Synchrotron Radiation Crystallography", Coppens, P. (Ed.), Academic Press, (1992).

David, W. I. F., Ferroelasticity in Scheelit Structures, *Solid State Chemistry*, Proc. of the Second European Conf., Veldhoven, The Netherland, 7-9, June (1982). Edited by Metselaar, R., Heijligers, H. J. M. and Schoonman, J. *Studies in Inorganic Chemistry* Vol. 3, P. 805, (1983).

Dokko, P. C. Pask, J. A. and Masdiyasni, K. S. J. Am. Ceram. Soc., 60 [3-4] 150 (1977).

Cameron, W. E. ., Am. Mineral., 62 [11] 747 (1977).

Dean, C., An Interactive Program for Crystal Orientation and Martensitic Transformation Investigations: COATI, *J. Appl. Cryst.* Vol. 18, p.159 (1985).

Dixon, R. D. , Chevacharoenkul, S. , Davis, and Tiegs, T. N. in Ceramic Transactions, edited by S. Somiya, R. F. Davis, and J. A. Pask (Am Ceram Soc., Westerville, OH, 1990) pp.579-603.

Engleman, M., 1993, FIDAP 7.0: Fluid Dynamics Analysis Package, FDI Inc., Evanston, IL.

Evans, A. G. and Cannon, R. M., Toughening of Brittle Solids by Martensitic Transformations," *Acta Metall.* Vol 34 [5] p.761 (1986).

Evans, A. G., Perspective on the Development of High-Toughness Ceramics, *J. Am. Ceram. Soc.,* vol.73 [2] p.187 (1990).

W. L. Fraser and S. W. Kennedy, The Crystal Structural Transformation NaCl-type ®CsCl-Type: Analysis by Martensite Theory, Acta. Crystallogr. Sect. A. Vol. 30, p.13 (1974).

Frazer, C. S., Dickey, E. C. , and Sayir, A. "Crystallographic Texture and Orientation Variants in Al_2O_3-$Y_3Al_5O_{12}$ Directionally Solidified Eutectic Crystals, accepted for publication in J. Crystal Growth, (2001).

Feigelson, R. S. MRS Bull., [10] 47 (1988).

Ferguson, R. B., The Crystallography of Synthetic $YTaO_4$ and Fused Fergusonite, Canad. Mineral. Vol. 6 p.72 (1957).

Garvie, R. C., Hannink, R. H. and Pascoe, R. T. , Ceramic Steel?, *Nature* vol. 258 p. 703 (1975).

Green, D. J., Hannink, R. H. J., and Swain, M. V., Transformation Toughening of Ceramics, CRC Press, Boca Raton, Florida (1989).

Glasser, F. P. , Warshaw, I. and Roy, R. , Phy. Chem. Glasses, 1, 39 (1960).

Galakhov F. Y. , and Konovalova, S. F. Bull. Acad. Sci. USSR Div. Chem. Sci. 8 1373 (1964)

Heuer, A. H. and Hobbs, L. W. , Eds. Science and Technology of Zirconia I in *Advances in Ceramics*, vol. 3. Publ. by the American Ceramic Society, Columbus, Oh, USA (1981).

Heuer, A. H. and Rühle, M., On the Nucleation of the Martensitic Transformation in Zirconia (ZrO_2), *Acta Metall.* Vol. 33 [12] p. 2101 (1985).

Hubert, J., Revcolevschi, A. and Collongues, R., "Application du chaffage par concentration de rayonnement (four à image) à la diffraction des rayons X à trés haute température (3200°)", *Can. Metall. Q.,* Vol. 13, p.361 (1974).

Holm, J. L. and Kleppa, O. J. , Am. Mineral., 51 [11-12] 1608 (1966).

Humphreys, L. B. Heminger, . A. , and Young, G. W. , J. Cryst. Growth, [100] 31 (1990).

Huang, C. M., Xu, Y., Zhu, D., Kriven, W. M., Combustion -synthesized b´-SiAlON reinforced with SIC Monofilaments, *Mater. Sci. Eng. A* Vol.188 p341 (1994).

Ismail, M. G. M. U., , Nakai, Z. and Somiya, S. J. Am. Ceram. Soc., 70 [1] C7 (1987).

Jero, P. D. and Kriven, W. M., High Temperature Transformation Toughening of Magnesia by Terbia, in Science and Technology of Zirconia V. Technomic Publishing Co., p190 (1993).

Kriven, W. M. and Pask, J. A. , J. Am. Ceram. Soc., 66 [9] 649 (1983).

Kim, K. M. ,J. Appl. Phys., 50 [2] 1135 (1979).

Kim, K. M. Dreben, A. B. ,and Schujko, A. .,J. Appl. Phys., 50 [6] 4472 (1979) .

Kanzaki, S. , Tabata, H., Kumazawa, T. , and Ohta, S. , J. Am. Ceram. Soc., 68 [1] C6 (1985).

Kassemi, M. and Duval, W.M.B., Interaction of Surface Radiation with Convection in Crystal Growth by Vapor Transport, *J. Thermophysics and Heat Transfer,* Vol. 11, p. 454, (1990).

Kassemi, M. and Duval, W., 1989, Effect of Gas and Surface Radiation on Crystal Growth from the Vapor Phase, *PhysicoChemical Hydrodynamics,* Vol. 11, p. 737.

Kassemi, M., and Naraghi, M.H.N., 1993, Analysis of Radiation-Natural Convection Interactions in 1-g and Low-g Environments Using the Discrete Exchange Factor Method, *Int. J. Heat and Mass Transfer,* Vol. 36, No. 17, p. 4141.

Kuo, C. K. in Ceramic Transactions, edited by S. Somiya, R. F. Davis, and J. A. Pask (Am Ceram Soc., Westerville, OH, 1990) pp.51 - 58.

Klug, F. J. Prochazka S. and Doremus R. H., J. Am. Ceram. Soc., 70 [10] 750 (1987).

Kelly, A, and Groves, G. W., Crystallography and Crystal Defects, Longman Group Ltd., Ch. 8 (1970).

Kriven, W. M., Fraser, W. L. and Kennedy, S. W., The Martensite Crystallography of Tetragonal Zirconia, in Science and Technology of Zirconia I. Heuer, A. H. and Hobbs, L. W. , Eds. *Advances in Ceramics,* vol. 3, p. 82. Publ. by the American Ceramic Society, Columbus, Oh, USA (1981).

Kriven, W. M., The Transformation Mechanism of Spherical Zirconia Particles in Alumina, in Science and Technology of Zirconia II in *Advances in Ceramics,* vol. 12., p64. Claussen, N., Rühle, M. and Heuer, A. H. , Eds. Publ. by the American Ceramic Society, Columbus, Oh, USA (1984).

Kriven, W. M., Possible Alternative Transformation Tougheners to Zirconia: Crystallographic Aspects, *J. Am. Ceram. Soc.,* vol. 71 [12] p.1021 (1988).

Kriven, W. M., Twinning in Structural Ceramics, in Twinning in Advanced Materials, ed. M. H. Yoo and M. Wuttig. Publ. The Minerals, Metals and Materials Society (TMS), Warrendale, PA, p. 435 (1994).

Kriven, W. M. , Displacive Phase Transformations and their Applications in Structural Ceramics, *J. de Physique IV, Colloque* C8, Vol. 5 p C101 (1995).

Kriven, W. M. and Lee, S.-J., Mullite-Cordierite Laminates with b®aCristobalite Transformation Weakened Interphases, Cer. Eng. Sci. Proc. Vol. 19 [3] p 305 (1998).

Kriven, W. M. and Lee, S.-J., Toughening of Oxide Ceramics by Transformation Weakening of Interphases; *J. Am. Ceram. Soc.,* 2001, submitted.

Kriven, W. M., Huang, C. M., Zhu, D., and Y. Xu, Toughening of Titania by Transformation Weakening of Enstatite ($MgSiO_3$) Interphases, *Acta Metall. Mater.,* (2001) submitted.

Ledbetter, H. M. and Wayman, C. M., PROGRAM MRTNST, Mater. Sci. Eng. Vol. 7 p.151 (1971).

Lin, C., and Motakef, S., Modeling of Directional Solidification of BSO, *J. Crystal Growth,* Vol. 128, p. 834 (1993).

Lieberman, D. S., Read, T. A., and Wechsler, M. S., Graphical Analysis of Diffusionless Phase Changes - The Cubic to Twinned Orthorhombic Transformation, *J. Appl. Phys.,* vol.28, p.532, (1957).

Lieberman, D. S., Martensitic Transformations and Determination of the Inhomogeneous Shear, *Acta Met.* Vol. 6, p.680 (1958).

Lieberman, D. S., in Phase Transformations. Published by the American Society for Metals, p.1 (1968).

Mather, S. A. and Davies, P. K., Nonequilibrium Phase Formation in Oxide Prepared at Low Temperature: Ferfusonite-Related Phases, *J. Am. Ceram. Soc.,* Vol. 78 [10] p. 2737 (1995).

Müllner, P., and Kriven, W. M., On the Role of Deformation Twinning in Domain Reorganization and Reorientation in Ferroelastic Crystals," *J. Mater. Res.* Vol. 7 p.1771 (1997)

Mumme, W. G. and Wadsley, A. D. The Structure of Orthorhombic Y_2TiO_5, an Example of Mixed Seven- and Fivefold Coordination, *Acta Cryst.* Vol. B24, p. 1327 (1968).

Naraghi, M.H.N. and Kassemi, M., Analysis of Radiative Transfer in Rectangular Enclosures Using a Discrete Exchange Factor Method, ASME *J. Heat Transfer*, Vol 111, p. 1117 (1989).

Nishiyama, Z., Martensitic Transformation. Published by Academic Press, (1978).

O'Hara, S., Tarshis, L.A., and Viskanta R., Stability of the Solid-Liquid Interface of Semi-Transparent Materials, *J. Crystal Growth,* Vol. 3-4, p. 583 (1968).

Pisarenko, G. G., Chushko, V. M. and Kovalev, S. P., Anisotropy of Fracture Toughness of Piezoelectric Ceramics, *J. Am. Ceram. Soc.* Vol. 68 [5] p. 259 (1985).

Petrova, M. A., Romanov, D. P., Rakhmankulov, R. M. Novikova, A. S. and Grebenshchikov, R. G., The Synthesis and X-ray Diffraction Study of Single Crystals of Dy_2TiO_5, *Russian Journal of Inorganic Chemistry* Vol. 31 [5] p. 761 (1986).

Petrova, M. A., Novikova, A. S., and Grebenshchikov, Polymorphism of Rare Earth Titanates of the Composition Ln_2TiO_5, Translated from *Izvestiya Akademii Nauk SSSR, Neorganischeskie Materialy*, Vol. 18, [2] p. 287 (1982).

Petrova, M. A. and Novikova, Crystallochemical Classification of Rare Earth Oxyorthotitanates, Translated from *Izvestiya Akademii Nauk SSSR, Neorganischeskie Materialy*, Vol. 15, [8] p. 1425 (1979).

Pohanka, R. C, Freiman, S. W. and Bender, B. A., Effect of Phase Transformation on the Fracture Behavior of $BaTiO_3$, *J. Am. Ceram. Soc.* Vol.61 [1] p.72 (1978).

Pohanka, R. C., Freiman, S. W. and Rice, R. W., Fracture Processes in Ferroic Materials, *Ferroelectrics* vol. 28, p. 337 (1980).

Quinn, C., and Wusirika, R., Twinning in $YNbO_4$ *J. Am. Ceram. Soc.,* Vol. 74 [2] p. 431 (1991).

Singh, A.K., Mao, H-K ., Shu, J. and Hemley, R.J. Estimation of Single-crystal Moduli from Polycrystalline X-ray Diffraction at High Pressure: Application to FeO and Iron., *Phys. Rev. Lett.* Vol. 80, p. 2157 (1998).

Saltiel, C., and Naraghi, M.H.N., 1990, Combined-Mode Heat Transfer in Radiatively Participating Media Using the Discrete Exchange Factor Method with Finite Elements, Heat Transfer 1990, Hemisphere Publication, Vol. 6, pp. 391-396.

Sayir, A., and Farmer, S. C., "Directionally Solidified Mullite Fibers," in Ceramic Matrix Composites-Advanced High TemperatureStructural Materials, eds., R. A. Lowden, M. K. Ferber, J. R. Hellmann, K. K. Chawla, and Stephen G. DiPietro, Mat. Res. Proc., Vol. 365 p. 11 (1995).

Sayir, A., "Directional Solidification of Eutectic Ceramics," in *Computer-Aided Design of High-Temperature Materials*. Eds. A. Pechenik, R.K. Kalia, P. Vashista, Oxford University Press p.197 (1999).

Sayir, A., and S. C. Farmer, The Effect of the Microstructure on Mechanical Properties of Directionally Solidified $Al_2O_3/ZrO_2(Y_2O_3)$ Eutectic," Acta. Mater., Vol. 48, p. 4691 (2000).

Sayir, A., and Farmer, S. C., "Fracture Characteristics of Single Crystal and Eutectic Fibers,' in print in *Fibre Fracture*, Elsevier Science, (2001).

Schneider, J., Mirror Heaters for High-temperature X-ray Diffraction" *Adv. X-ray Analysis*, Vol. 36, p. 397 (1993).

Shamrai, G. V., Magunov, R. L., Stasenko, I. V. and Zhirnova, A. P., The Dy_2O_3 - TiO_2 System, Translated from *Izvestiya Akademii Nauk SSSR, Neorganischeskie Materialy*, Vol. 25, [2] p. 237 (1989).

Shcherbakova, L. G., Mamsurova, L. G., and Sukhanova, G. E., Lanthanide Titanates, *Russian Chemical Reviews* Vol. 48 [3] p. 228 (1979). Translated from *Uspekhi Khimii,* Vol. 48 p.423 (1979).

Sinogeikin, S.V., and Bass, J.D., Single Crystal Elasticity of Pyrope and MgO to Pressures of 20 GPa by Brillouin Scattering in the Diamond Cell, Phys. Earth Planet. Interiors Vol.120,p. 43 (2000).

Stecura, S., Evaluation of an imaging furnace as a heat source for X-ray diffractometry, *Rev. Sci. Instrum.*, Vol. 39, p.760 (1968).

Stubican, V. S., High Temperture Transitions in Rare-Earth Niobates and Tantalates, *J. Am. Ceram. Soc.* Vol. 47 [2] p. 55 (1964).

Sudre, O., Venkatachari, and Kriven, W. M., Kinetics and Crystallography of the Monoclinic (B) to (C) Transformation in Dysprosia, in Science and Technology of Zirconia V. Technomic Publishing Co., p180 (1993).

Sukhanova, G. E., Guseva, K. N., Mamsurova, L. G., and Shcherbakova, L. G., Structural Transitions of Rare Earth Titanates. Translated from Izvestiya Akademii Nauk SSSR, Neorganischeskie Materialy Vol. 17, [6] p.1043 (1981).

Tarshis, L.A., O'Hara, S. and Viskanta R., Heat Transfer by Simultaneous Conduction and Radiation for two Absorbing Media in Intimate Contact, *Int. J. Heat Mass Transfer*, Vol. 12, p. 333 (1969).

Virkar, A. V., and Matsumoto, R. L. K., Ferroelastic Domain Switching as a Toughening Mechanism in Tetragonal Zirconia, *J. Am. Ceram. Soc.,* Vol. 69 [10] p C224 (1986).

Virkar, A. V., Jue, J. F., Smith, P., Mehta, K., and Prettyman, K., The Role of Ferroelasticity in Toughening of Brittle Materials, *Phase Transitions* Vol. 35 p.27 (1991).

Viskanta, R., and Anderson E.E., Heat Transfer in Semitransparent Solids, *Advances in Heat Transfer*, (Eds T.F. Irvine and J.P. Hartnett, Academic Press), Vol. 11, p. 318 (1975).

Witt, A. F., 1993, Personal Communication.

Wadhawan, V. K., "Ferroelasticity and Related Properties of Crystals, *Phase Transitions* vol 3, p.3 (1982).

Wadhawan, V.K., Practical Signficance of the Ferroelastic Nature of the Superconductor Y-Ba-Cu-O", *Ferroelectrics*, Vol. 97 p. 171 (1989).

Watanabe, A. and Shimazu, M., "High-temperature X-ray diffraction furnace using a thermal-image technique", *J. Appl. Cryst.*, Vol. 9, p. 466 (1976).

Wayman, C. M., <u>Introduction to the Crystallography of Martensitic Transformations</u>, Macmillan publishers, New York, (1964).

Wechsler, M. S., D. S. Lieberman and Read., T. A, On the Theory of the Formation of Martensite, AIME Trans., Vol.197 p 1503. (1953).

Wechsler, M. S., Read, T. A. and Lieberman, D. S., The Crystallography of the Austenite-Martensite Transformation. The {111} Shear Solutions. Trans. AIME. Vol 218, p. 202, (1960.

Wolten, G. M., The Structure of the M′-Phase of $YTaO_4$, a Third Fergusonite Polymorph, *Acta Cryst.* Vol. 23, p.939 (1967).

Yuferev, V.S. and Vasil'ev, M.G., Heat Transfer in Shaped Thin-Walled Semitransparent Crystals Pulled from the Melt, *J. Crystal Growth*, Vol. 82, p. 31 (1987).